PHYSICAL REVIEW E **91**, 012709 (2015)

Fluid flow enhances the effectiveness of toxin export by aquatic microorganisms: A first-passage perspective on microvilli and the concentration boundary layer

Nicholas A. Licata* and Aaron Clark
Department of Natural Sciences, University of Michigan–Dearborn, Dearborn, Michigan 48128, USA
(Received 17 September 2014; published 26 January 2015; corrected 5 August 2015)

A central challenge for organisms during development is determining a means to efficiently export toxic molecules from inside the developing embryo. For aquatic microorganisms, the strategies employed should be robust with respect to the variable ocean environment and limit the chances that exported toxins are reabsorbed. As a result, the problem of toxin export is closely related to the physics of mass transport in a fluid. In this paper, we consider a model first-passage problem for the uptake of exported toxins by a spherical embryo. By considering how macroscale fluid turbulence manifests itself on the microscale of the embryo, we determine that fluid flow enhances the effectiveness of toxin export as compared to the case of diffusion-limited transport. In the regime of a large Péclet number, a perturbative solution of the advection-diffusion equation reveals that a concentration boundary layer forms at the surface of the embryo. The model results suggest a functional role for cell surface roughness in the export process, with the thickness of the concentration boundary layer setting the length scale for cell membrane protrusions known as microvilli. We highlight connections between the model results and experiments on the development of sea urchin embryos.

DOI: 10.1103/PhysRevE.91.012709 PACS number(s): 87.16.dp, 47.63.mh, 47.27.T−

I. INTRODUCTION

Aquatic organisms face a variety of challenges in the course of their development. Central challenges related to their growth and development are the acquisition of nutrients from the surrounding fluid and the disposal of waste products or other toxic materials to the extracellular environment. As a result, aquatic organisms have evolved a diverse set of strategies to search for, acquire, and dispose of small molecules. Successful strategies reflect fundamental constraints imposed by the physical laws that govern the transport and motion of small particles in a fluid. This line of physical reasoning has shaped our understanding of a variety of problems in biology, from bacterial chemotaxis [1,2] to the origin of multicellularity in algae [3,4].

The present paper highlights a connection between the physics of mass transport in a fluid flow and the problem of removing toxic molecules or other waste products from a developing embryo. The major question addressed can be stated quite simply. A spherical embryo has identified a toxic molecule for export to the extracellular fluid. Once exported, the molecule will be subject to diffusion and advection in the surrounding fluid. How far away from the body of the embryo should the molecule be released, so as to reduce the chances that the toxin encounters the embryo surface and is reabsorbed? The view advocated in the present paper is that the physics underlying this transport problem provides an answer that may shed light on understanding the functional role of cell surface roughness in embryonic development. Later we will argue that the length of cell surface protrusions known as microvilli (the surface roughness elements implicated in the toxin export process) may be determined in part by the thickness of the concentration boundary layer for the advection-diffusion problem.

*Author to whom all correspondence should be addressed: licata@umich.edu

The interplay between the thickness of the concentration boundary layer and the size and functional significance of biological structures has been documented in a variety of cases [5]. In particular, our results are probably closest conceptually to the findings of Short *et al.* on the role of fluid flow in enhancing nutrient uptake by *Volvox carteri* [4]. In that work, it was demonstrated that beyond a critical bottleneck radius, diffusion alone is insufficient to meet the metabolic needs of a growing algae colony. By actively stirring the fluid, the colony is able to overcome this nutrient deficiency. The concentration boundary layer thickness is comparable to the length of flagella, the stirring rods responsible for fluid mixing.

In the present case of sea urchin embryogenesis, several recent experiments have highlighted the important role that cell surface roughness plays in toxin export. Early in sea urchin development, microvilli lengthen, and there is a coincident localization of transport receptors to the tips of the microvilli [6,7]. These transport receptors act to export toxic molecules from the interior of the cell to the extracellular fluid [8,9]. This suggests that the localization of transport receptors to the tips of the microvilli may serve a functional role in the export process. Releasing the toxic molecules at a distance h (the microvilli length) from the cell membrane surface may reduce the chances that exported toxins are subsequently reabsorbed by the cell.

In this paper, we investigate the efficacy of the tip localization strategy by considering a model first-passage problem [10] for the uptake of exported toxins by a spherical embryo. In Sec. II we consider the regime of diffusion-limited transport. We demonstrate that tip localization does not confer a significant advantage to the embryo in this case. In general, the transport of toxic molecules in the extracellular fluid will depend not only on diffusion, but also on fluid advection. We quantify the fluid flow surrounding the embryo in Sec. III. In Sec. IV we discuss the concentration boundary layer that forms when the toxin is advected along with the flow. We revisit the first-passage problem in the case of strong advection in Sec. V. A perturbative solution of the advection-diffusion

equation in the regime of a large Péclet number reveals that fluid flow enhances the effectiveness of the tip localization strategy. In Sec. VI we discuss the effect of surface roughness on the first-passage probability. We conclude in Sec. VII by highlighting connections between the model results and recent experiments on the development of sea urchin embryos.

II. THE CASE OF PURE DIFFUSION

Consider a spherical embryo of radius $R \sim 40\ \mu$m. In the absence of fluid flow, a toxin released from the tip of a microvilli will diffuse in the extracellular fluid. The diffusion coefficient of the toxin in the extracellular fluid is $D \sim 10^{-5}$ cm^2 s^{-1}, characteristic of small molecules in water. The goal is to determine the probability that a released toxin will be reabsorbed by the cell. In this paper, we consider the case of a perfect spherical absorber. This approximation is not as severe as one might imagine, as the perfectly absorbing sphere is a relatively good approximation to the case of a patchy reactive surface [1]. In what follows, we do not treat the chemical kinetics associated with the absorption process. For a discussion of toxin transport in the sea urchin embryo that includes chemical kinetics, see Chapter 5 of [11]. In the model formulation, all molecules that reach the cell surface are absorbed. This constitutes a *worst* case scenario for the cell. As a result, the first-passage probability calculated will set an upper bound on the true absorption probability. In addition, at the outset we will ignore reabsorption by the microvilli themselves, and only consider absorption by the spherical surface. In this approximation, the only role of the microvilli is to release the toxin molecules at a distance h above the surface of the cell. In Sec. VI we will revisit this approximation and discuss the role of surface roughness on the absorption probability in more detail.

The toxin concentration C satisfies the diffusion equation

$$\frac{\partial C}{\partial t} = D\nabla^2 C. \tag{1}$$

Defining the dimensionless length $\xi = r/R$, concentration $c = R^3 C$, and time $\tau = (Dt)/R^2$ yields

$$\frac{\partial c}{\partial \tau} = \nabla_\xi^2 c. \tag{2}$$

$\nabla_\xi^2 c = \frac{1}{\xi^2}\frac{\partial}{\partial \xi}(\xi^2 \frac{\partial c}{\partial \xi}) + \frac{1}{\xi^2 \sin\theta}\frac{\partial}{\partial \theta}(\sin\theta \frac{\partial c}{\partial \theta}) + \frac{1}{\xi^2 \sin^2\theta}\frac{\partial^2 c}{\partial \phi^2}$ denotes the Laplacian with respect to the dimensionless radial variable ξ. Considering the Laplace transform of the concentration $\tilde{c} = \int_0^\infty e^{-s\tau} c\, d\tau$ gives the partial differential equation

$$\nabla_\xi^2 \tilde{c} - s\tilde{c} = -c(\tau = 0) = -\delta^3(\vec{\xi} - \vec{\xi}'). \tag{3}$$

The initial condition corresponds to a point source at the microvilli tip, and it reveals that the Laplace transform of the concentration is the Green's function for the modified Helmholtz operator. A solution in spherical polar coordinates can be obtained by introducing the expansion

$$\tilde{c} = \sum_{\ell=0}^{\infty}\sum_{m=-\ell}^{\ell} a_{\ell m}(\xi,\xi') Y^*_{\ell m}(\theta',\phi') Y_{\ell m}(\theta,\phi). \tag{4}$$

The resulting radial equation for $a_{\ell m}(\xi,\xi')$ is solved with the absorbing boundary condition at the cell surface, $a_{\ell m}(\xi = 1,\xi') = 0$, and requiring the solution to be finite at infinity. The solution can be expressed in terms of the spherical modified Bessel functions [12] $i_\ell(x) = \sqrt{\frac{\pi}{2x}} I_{\ell+1/2}(x)$ and $k_\ell(x) = \sqrt{\frac{2}{\pi x}} K_{\ell+1/2}(x)$ as

$$a_{\ell m}(\xi,\xi') = \gamma k_\ell(\gamma\xi_>)\left[i_\ell(\gamma\xi_<) - \frac{i_\ell(\gamma)}{k_\ell(\gamma)} k_\ell(\gamma\xi_<)\right], \tag{5}$$

where $\gamma^2 = s$. Here $\xi_<$ ($\xi_>$) represents the smaller (larger) of ξ and ξ'. The first-passage probability is determined from the time integral of the diffusive current density impinging on the sphere surface,

$$\Pi_D = \int_0^\infty dt \iint \vec{J}\cdot d\vec{a}. \tag{6}$$

Evaluating $\vec{J}\cdot d\vec{a} = D\frac{\partial C}{\partial r}|_{r=R} R^2 \sin\theta\, d\theta\, d\phi$ on the surface of the sphere, the first-passage probability can be written simply in terms of the Laplace transform of the dimensionless concentration,

$$\Pi_D = \lim_{s\to 0}\int_0^\pi \sin\theta\, d\theta \int_0^{2\pi} d\phi \left.\frac{\partial \tilde{c}}{\partial \xi}\right|_{\xi=1} = \frac{1}{\xi'}. \tag{7}$$

This remarkably simple and well-known result [10] is illustrated in Fig. 1. The details of the derivation are outlined in Appendix A. The result indicates that, in the case of pure diffusion, tip localization is not a very effective strategy for reducing the chances that exported toxins get reabsorbed. In the dimensionless coordinates, the tip of the microvilli is located at $\xi' = 1 + \frac{h}{R}$. With microvilli of length $h \sim 2\ \mu$m and an embryo of radius $R \sim 40\ \mu$m, the absorption probability is $\Pi_D = 0.95$. Examining the structure of the microvilli solely through the lens of toxin export, if transport were diffusion-limited, one might expect significantly longer microvilli than what is observed experimentally.

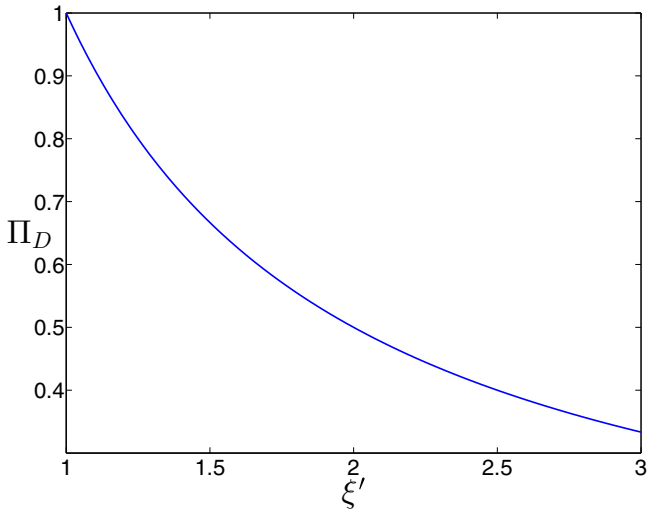

FIG. 1. (Color online) The first-passage probability Π_D as a function of the microvilli tip location $\xi' = 1 + \frac{h}{R}$ for the case of pure diffusion. The microvilli have length h and the embryo has radius R.

III. FLUID FLOW

In reality, the transport of toxins in the extracellular fluid is determined not only by diffusion, but also by advection. The dimensionless Péclet number Pe characterizes the competition between advection and diffusion,

$$\mathrm{Pe} = \frac{RU_0}{D}. \tag{8}$$

Here U_0 is a characteristic flow velocity, which will be discussed in more detail shortly. We define the dimensionless fluid velocity as $\vec{u} = \frac{\vec{U}}{U_0}$. For an incompressible fluid $\vec{\nabla}_\xi \cdot \vec{u} = 0$, and the dimensionless toxin concentration satisfies

$$\frac{\partial c}{\partial \tau} + \mathrm{Pe}\,\vec{u} \cdot \vec{\nabla}_\xi c = \nabla_\xi^2 c. \tag{9}$$

An important property of the fluid flow is the Reynolds number

$$\mathrm{Re} = \frac{RU_0}{\nu}, \tag{10}$$

where $\nu \sim 10^{-6}$ m^2 s^{-1} is the kinematic viscosity of ocean water. To proceed, we investigate the nature of the fluid flow in the vicinity of the embryo. In particular, the wave-swept rocky shore that is the habitat for the sea urchin is an environment where turbulent mixing takes place on the macroscale [13,14]. The question is how this turbulence manifests itself on the microscale of the embryo [15–17]. Kolmogorov's first similarity hypothesis states that small-scale fluid motion is universal and determined by two parameters, namely the kinematic viscosity ν (m^2 s^{-1}) and the turbulent kinetic energy dissipation rate ε (m^2 s^{-3}). The unique length $\eta = (\nu^3/\varepsilon)^{1/4}$ and time $\tau_\eta = (\nu/\varepsilon)^{1/2}$ scales characterize the smallest dissipative eddies in the flow [18]. In particular, the size of the smallest turbulent eddies is $\sim 2\pi\eta$ [15]. As a result, the smallest eddies are at least an order of magnitude larger than the embryo, and the local fluid environment of the embryo is one characterized by velocity gradients $\sim 1/\tau_\eta$.

To calculate the first-passage probability, we need to specify the specific form of the fluid velocity appearing in Eq. (9). In what follows, we will work with the model introduced earlier by Batchelor [19,20]. The model is applicable in the present case because Re $\ll 1$, and we are considering the case of an isolated embryo. For the calculation, only the fluid velocity relative to the embryo matters. This velocity is due in part to the motion of the embryo through the fluid as a result of an applied force and in part due to the ambient motion of the fluid, which would be present even in the absence of the embryo. The former takes into account gravity and includes the effect of buoyancy, since in general the density of the embryo will differ from that of the fluid. One expects that in an otherwise quiescent fluid, this density mismatch would lead a nonmotile embryo to sink under the influence of gravity. This behavior is observed experimentally in sea urchin embryos. For example, the sinking velocity of *Strongylocentrotus purpuratus* is $V \sim 0.4$ mm s^{-1} [21]. Interestingly, this is comparable to the embryo's swimming velocity later in development. The second contribution to the fluid velocity stems from the universal small-scale motion of the fluid as a result of turbulent dissipation discussed above. These two sources make independent contributions to the fluid velocity in the vicinity of the embryo. Relative to the velocity of the embryo center, the fluid velocity $\vec{U}$ can be expressed as [20]

$$\vec{U} = \vec{V} \cdot \left[\left(\frac{3}{4\xi} + \frac{1}{4\xi^3} - 1\right)\mathsf{I} + \left(\frac{3}{4\xi} - \frac{3}{4\xi^3}\right)\vec{\xi}\,\vec{\xi}\,\right] + R\,\Omega \cdot \vec{\xi} + R\,\vec{\xi} \cdot \mathsf{E} \cdot \left[\left(1 - \frac{1}{\xi^5}\right)\mathsf{I} - \frac{5}{2}\frac{1}{\xi^3}\left(1 - \frac{1}{\xi^2}\right)\vec{\xi}\,\vec{\xi}\,\right]. \tag{11}$$

Here I is the unit tensor. The first term accounts for the aforementioned sinking behavior due to gravity and the disturbance motion this generates in the flow. As for the contribution from the ambient fluid motion (subscript a for ambient), the velocity gradient tensor $\vec{\nabla}\vec{U}_a = \mathsf{E} + \Omega$ corresponds to the ambient fluid motion and has been decomposed into its symmetrical (E) and antisymmetrical (Ω) parts. The antisymmetric part $\Omega_{ij} = -\frac{1}{2}\epsilon_{ijk}\omega_k$ represents the rigid body rotation of the embryo with angular velocity $\frac{1}{2}\vec{\omega}$, where $\vec{\omega} = \vec{\nabla} \times \vec{U}_a$ is the vorticity of the ambient flow [19]. Here ϵ_{ijk} is the Levi-Civita symbol. As discussed in [20], in the low Reynolds number regime the embryo will rotate with the ambient fluid at all times. In contrast, the embryo cannot follow the straining motion of the ambient fluid represented by the symmetric rate of strain tensor E, which generates a disturbance motion in the flow.

This motivates defining the characteristic velocity $U_0 = (R\omega)/2$ and hence the associated Reynolds number,

$$\mathrm{Re} = \frac{R^2\omega}{2\nu}, \tag{12}$$

and the Péclet number,

$$\mathrm{Pe} = \frac{R^2\omega}{2D}. \tag{13}$$

The microscale velocity gradient is related to the angular velocity as $1/\tau_\eta = \omega/2$. We note that there is a great deal of variation, both spatial and temporal, in the value of ε and hence ω. A characteristic value for the upper mixed layer of the ocean might be $\varepsilon \sim 10^{-6}$ m^2 s^{-3} [15–17], whereas an embryo in a surge channel might be subject to instantaneous values a million times larger, $\varepsilon \sim 1$ m^2 s^{-3} [13,14]. Using the value of the kinematic viscosity of ocean water, ν, and an appropriate range of values for the kinetic energy dissipation rate, ε, one can see from Fig. 2 that the regime of interest is one in which Re $\ll 1$, but Pe $\gg 1$. Note that the condition Re $\ll 1$ justifies the choice of a model in which the fluid velocity is obtained as a solution of the Stokes equation.

In what follows, we will calculate the first-passage probability perturbatively, making use of the fact that the quantity $\alpha = 1/\mathrm{Pe} \ll 1$. In spherical polar coordinates, the resulting partial differential equation for the dimensionless concentration Eq. (9) is

$$\alpha\frac{\partial c}{\partial \tau} + u_\xi\frac{\partial c}{\partial \xi} + \frac{u_\theta}{\xi}\frac{\partial c}{\partial \theta} + \frac{u_\phi}{\xi\sin\theta}\frac{\partial c}{\partial \phi} = \alpha\nabla_\xi^2 c. \tag{14}$$

The dimensionless velocity components ($\vec{u} = \vec{U}/U_0$ and $\vec{v} = \vec{V}/U_0$) can be calculated as

$$u_\xi = (A + B)v_\xi + (F - G)\mathsf{e}_{\xi\xi}, \tag{15}$$

$$u_\theta = Av_\theta + F\mathsf{e}_{\xi\theta}, \tag{16}$$

$$u_\phi = Av_\phi + \xi\sin\theta + F\mathsf{e}_{\xi\phi}. \tag{17}$$

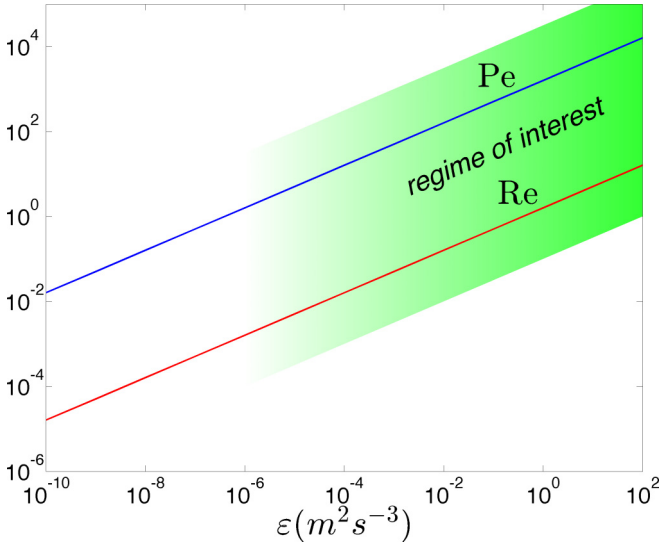

FIG. 2. (Color online) The dimensionless Péclet number Pe (blue line) and Reynolds number Re (red line) as a function of the turbulent kinetic energy dissipation rate ε ($\mathrm{m^2\,s^{-3}}$).

Here we have introduced the shorthand notation

$$A = \frac{3}{4\xi} + \frac{1}{4\xi^3} - 1, \tag{18}$$

$$B = \frac{3}{4\xi}\left(1 - \frac{1}{\xi^2}\right), \tag{19}$$

$$F = \xi - \frac{1}{\xi^4}, \tag{20}$$

$$G = \frac{5}{2\xi^2}\left(1 - \frac{1}{\xi^2}\right). \tag{21}$$

In addition, we have introduced the dimensionless velocity gradient tensor $\vec{\nabla}_\xi \vec{u}_a = \mathsf{e} + \psi$ with $\vec{u}_a = \vec{U}_a/U_0$, $\mathsf{e} = \frac{R}{U_0}\mathsf{E}$, and $\psi = \frac{R}{U_0}\Omega$. Note that the rotation of the embryo with the ambient fluid corresponds to $\Omega_{\phi r} = \frac{1}{2}\omega \sin\theta$ and hence $\psi_{\phi r} = \sin\theta$.

The small quantity α multiplying the highest order spatial derivative in Eq. (14) is the hallmark of a boundary layer problem. Physically this is an indication that the toxin concentration changes from its far-field value to the value $c = 0$ at the surface of the embryo ($\xi = 1$) in a thin concentration boundary layer in the vicinity of the surface. A piece of information of central importance to the current study is the dependence of the concentration boundary layer thickness on the Péclet number Pe, which was a result originally obtained by Lévêque in 1928 [22]. We will discuss this result in much greater detail in Sec. IV.

Within the concentration boundary layer, the dominant fluid motion is an azimuthal rotation, which corresponds to a solid body rotation of the embryo with the ambient fluid. Superimposed on top of this rotation is a small fluctuation. To proceed with the analysis, we move to a reference frame rotating with the embryo, denoting the fluid velocity components in this frame by $\overset{*}{u}_\gamma$ with $\gamma \in \{\xi,\theta,\phi\}$. The velocity components in the rotating frame can be obtained by removing the term $\xi \sin\theta$ from u_ϕ, and making the replacement $\phi \to \phi - \mathrm{Pe}\,\tau$. In the rotating frame, defining a Cartesian coordinate system (x_1,x_2,x_3) with the x_3 direction along the direction of the ambient vorticity, the velocity components are obtained from the following relations:

$$\overset{*}{v}_\xi = v_1 \sin\theta\cos(\phi - \mathrm{Pe}\,\tau) + v_2 \sin\theta \sin(\phi - \mathrm{Pe}\,\tau) + v_3 \cos\theta, \tag{22}$$

$$\overset{*}{v}_\theta = v_1 \cos\theta\cos(\phi - \mathrm{Pe}\,\tau) + v_2 \cos\theta \sin(\phi - \mathrm{Pe}\,\tau) - v_3 \sin\theta, \tag{23}$$

$$\overset{*}{v}_\phi = -v_1 \sin(\phi - \mathrm{Pe}\,\tau) + v_2 \cos(\phi - \mathrm{Pe}\,\tau), \tag{24}$$

$$\begin{aligned}\overset{*}{\mathsf{e}}_{\xi\xi} = {} & \mathsf{e}_{11}\sin^2\theta\cos^2(\phi - \mathrm{Pe}\,\tau) + \mathsf{e}_{22}\sin^2\theta\sin^2(\phi - \mathrm{Pe}\,\tau) \\ & + \mathsf{e}_{33}\cos^2\theta + \mathsf{e}_{12}\sin^2\theta\sin[2(\phi - \mathrm{Pe}\,\tau)] \\ & + \mathsf{e}_{13}\sin(2\theta)\cos(\phi - \mathrm{Pe}\,\tau) \\ & + \mathsf{e}_{23}\sin(2\theta)\sin(\phi - \mathrm{Pe}\,\tau),\end{aligned} \tag{25}$$

$$\begin{aligned}\overset{*}{\mathsf{e}}_{\xi\theta} = {} & \cos(2\theta)[\mathsf{e}_{13}\cos(\phi - \mathrm{Pe}\,\tau) + \mathsf{e}_{23}\sin(\phi - \mathrm{Pe}\,\tau)] \\ & + \frac{1}{4}\sin(2\theta)\{\mathsf{e}_{11} + \mathsf{e}_{22} - 2\mathsf{e}_{33} + (\mathsf{e}_{11} - \mathsf{e}_{22}) \\ & \times \cos[2(\phi - \mathrm{Pe}\,\tau)] + 2\mathsf{e}_{12}\sin[2(\phi - \mathrm{Pe}\,\tau)]\},\end{aligned} \tag{26}$$

$$\begin{aligned}\overset{*}{\mathsf{e}}_{\xi\phi} = {} & \cos\theta[\mathsf{e}_{23}\cos(\phi - \mathrm{Pe}\,\tau) - \mathsf{e}_{13}\sin(\phi - \mathrm{Pe}\,\tau)] \\ & + \mathsf{e}_{12}\sin\theta\cos[2(\phi - \mathrm{Pe}\,\tau)] \\ & + \tfrac{1}{2}(\mathsf{e}_{22} - \mathsf{e}_{11})\sin[2(\phi - \mathrm{Pe}\,\tau)].\end{aligned} \tag{27}$$

In principle, the quantities v_i, e_{ij} ($\{i,j\} \in \{1,2,3\}$), and Pe are functions of time, fluctuating over a time scale $\tau \sim 1/\mathrm{Pe}$ corresponding to the eddy turnover. Following Batchelor [20], we calculate the average velocity field in the vicinity of the embryo by averaging over a time scale $\tau_{\mathrm{long}} \gg 1/\mathrm{Pe}$ that is long compared to the fluctuation time scale,

$$\langle \overset{*}{u}_\gamma \rangle = \frac{1}{\tau_{\mathrm{long}}}\int_0^{\tau_{\mathrm{long}}} \overset{*}{u}_\gamma \, d\tau. \tag{28}$$

Assuming that v_i, e_{ij}, and Pe are stationary random functions of τ, the average of many terms is zero, like $v_i \cos(\phi - \mathrm{Pe}\,\tau)$ and $\mathsf{e}_{ij}\sin(\phi - \mathrm{Pe}\,\tau)$. The result for the averaged components is

$$\langle \overset{*}{v}_\xi \rangle = \langle v_3 \rangle \cos\theta, \tag{29}$$

$$\langle \overset{*}{v}_\theta \rangle = -\langle v_3 \rangle \sin\theta, \tag{30}$$

$$\langle \overset{*}{v}_\phi \rangle = 0, \tag{31}$$

$$\langle \overset{*}{\mathsf{e}}_{\xi\xi} \rangle = \langle \mathsf{e}_{33} \rangle, \tag{32}$$

$$\langle \overset{*}{\mathsf{e}}_{\xi\theta} \rangle = -\tfrac{3}{4}\sin(2\theta)\langle \mathsf{e}_{33} \rangle, \tag{33}$$

$$\langle \overset{*}{\mathsf{e}}_{\xi\phi} \rangle = 0. \tag{34}$$

Here we have invoked the statistical isotropy of the small-scale turbulence, and the incompressibility of the ambient fluid,

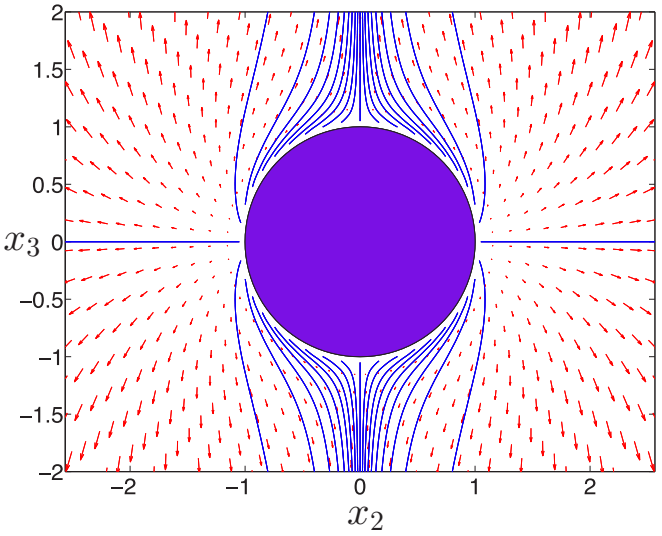

FIG. 3. (Color online) The time-averaged velocity field $\langle \vec{u}^* \rangle$ in the (x_2,x_3) plane (red arrows). Velocity streamlines starting at the tips of microvilli ($\xi' = 1.05$) are shown as blue lines.

$\mathsf{e}_{11} + \mathsf{e}_{22} + \mathsf{e}_{33} = 0$. As discussed in [20], $\langle v_3 \rangle = 0$. As a result, the time-averaged, dimensionless velocity field depends on a single parameter $\langle \mathsf{e}_{33} \rangle$, which for locally homogeneous and isotropic turbulence takes on the value $\langle \mathsf{e}_{33} \rangle \simeq 0.18$,

$$\langle u^*_\xi \rangle = (F - G)\langle \mathsf{e}_{33} \rangle, \tag{35}$$

$$\langle u^*_\theta \rangle = -\tfrac{3}{4} F \sin(2\theta)\langle \mathsf{e}_{33} \rangle, \tag{36}$$

$$\langle u^*_\phi \rangle = 0. \tag{37}$$

The enhancement of mass transfer in the case of strong advection is now clear. Within the concentration boundary layer, the average fluid flow consists of motion toward the north ($\theta < \pi/2$) or south ($\theta > \pi/2$) pole and a radial outflow (see Fig. 3). Toxin molecules released at the tips of microvilli will be advected away from the embryo, which will reduce their absorption probability.

IV. CONCENTRATION BOUNDARY LAYER

For the purpose of completeness and clarity, in this section we provide a pedagogical description of the concentration boundary layer phenomenon. Since boundary layers are a classic problem in fluid mechanics about which a great deal has been written, we will not attempt a general review of the subject, and instead we will restrict our discussion to the problem at hand. However, we note several references for the benefit of readers interested in the historical context of the subsequent mathematical development. The result for the concentration boundary layer thickness [Eq. (40)] dates to Lévêque [22], and the matched asymptotic analysis was originally presented in the context of Stokes flow by Acrivos and Taylor [23]. An introduction to the subject is presented in the book by Van Dyke [24]. A modern approach to the subject based on the perturbative renormalization group is presented by Chen, Goldenfeld, and Oono [25]. The paper of Veysey and Goldenfeld compares the renormalization group methodology to the matched asymptotic analysis, and it includes a wealth of information about the historical development of the subject [26].

In the present context, with the time-averaged velocity field as input, the advection-diffusion equation for the toxin concentration reads

$$\alpha \frac{\partial c}{\partial \tau} + \langle u^*_\xi \rangle \frac{\partial c}{\partial \xi} + \frac{\langle u^*_\theta \rangle}{\xi} \frac{\partial c}{\partial \theta} = \alpha \nabla^2_\xi c. \tag{38}$$

To investigate the quantitative implications of the boundary layer, we invoke the technique of dominant balance [25]. Namely, we determine a rescaling of the radial variable $\xi = 1 + \alpha^n \rho$ which stretches out the boundary layer. For the purposes of our first-passage calculation, we find it useful to rescale the dimensionless time as $\tau = \alpha^m T$, but not the angular variables θ and ϕ. At this point, the exponents n and m are unknown, but we are looking for a solution in which the lowest order governing equation for the concentration is independent of α and contains temporal, advective, and diffusive terms. The result of the rescaling is

$$\begin{aligned} \alpha^{2n-m} \frac{\partial c}{\partial T} + \alpha^{n-1} \langle u^*_\xi \rangle \frac{\partial c}{\partial \rho} + \frac{\alpha^{2n-1}}{(1+\alpha^n \rho)} \langle u^*_\theta \rangle \frac{\partial c}{\partial \theta} \\ = \frac{\partial^2 c}{\partial \rho^2} + \frac{2\alpha^n}{(1+\alpha^n \rho)} \frac{\partial c}{\partial \rho} + \frac{\alpha^{2n}}{(1+\alpha^n \rho)^2} \frac{1}{\sin\theta} \frac{\partial}{\partial \theta} \\ \times \left(\sin\theta \frac{\partial c}{\partial \theta} \right) + \frac{\alpha^{2n}}{(1+\alpha^n \rho)^2} \frac{1}{\sin^2\theta} \frac{\partial^2 c}{\partial \phi^2}. \end{aligned} \tag{39}$$

At this point, it is important to remember (see Appendix B) that when expressed in terms of the radial variable ρ, the velocity components $\langle u^*_\xi \rangle \sim O(\alpha^{2n})$ and $\langle u^*_\theta \rangle \sim O(\alpha^n)$ have nontrivial scaling with α. The correct choice of exponents for the rescaling is seen to be $n = 1/3$ and $m = 2/3$. In fact, the thickness of the concentration boundary layer, ℓ, is determined by the exponent n as (see Fig. 4) [22,23]

$$\ell = R\,\mathrm{Pe}^{-\frac{1}{3}}. \tag{40}$$

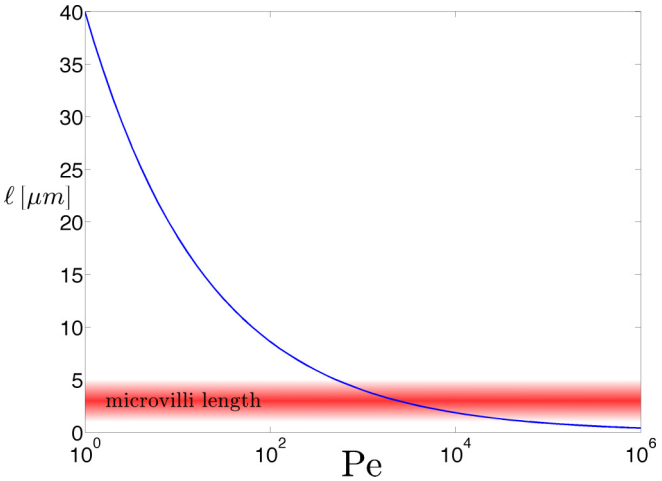

FIG. 4. (Color online) The concentration boundary layer thickness $\ell = R\,\mathrm{Pe}^{-\frac{1}{3}}$ as a function of Pe. At large Pe, the length of embryonic microvilli $h \approx \ell$.

We can now obtain a perturbative solution for the concentration in the form $c = \sum_{k=0}^{\infty} \alpha^{\frac{k}{3}} c_k$. Inserting this expansion into Eq. (39) and collecting terms of the same order in $\alpha^{\frac{1}{3}}$, one obtains a system of coupled equations for the $\{c_k\}$. Defining $\mu = \cos\theta$ and the parameter $\beta = \frac{15}{2}\langle \mathsf{e}_{33} \rangle$, the equations governing c_0 and c_1 are

$$\frac{\partial c_0}{\partial T} + \beta\rho^2 \frac{\partial c_0}{\partial \rho} + \beta\rho\mu(1-\mu^2)\frac{\partial c_0}{\partial \mu} - \frac{\partial^2 c_0}{\partial \rho^2} = 0, \quad (41)$$

$$\frac{\partial c_1}{\partial T} + \beta\rho^2 \frac{\partial c_1}{\partial \rho} + \beta\rho\mu(1-\mu^2)\frac{\partial c_1}{\partial \mu} - \frac{\partial^2 c_1}{\partial \rho^2} = \frac{8}{3}\beta\rho^3 \frac{\partial c_0}{\partial \rho} + 3\beta\rho^2\mu(1-\mu^2)\frac{\partial c_0}{\partial \mu} + 2\frac{\partial c_0}{\partial \rho}. \quad (42)$$

The perturbation program consists in calculating c_0 from Eq. (41), and using the solution to solve the inhomogeneous equation for c_1, Eq. (42). The solutions for c_1 and c_0 can then be utilized to calculate c_2, and so on [26]. Following the common practice in boundary layer problems [27,28], we define similarity variables $\eta = \rho/g$ and $\chi = T/g^2$, where the positive function $g(\mu)$ captures the angular dependence of the boundary layer. In terms of this similarity transformation, the zeroth-order equation becomes

$$\frac{\partial c_0}{\partial \chi} + \beta\eta^2\left(g^3 - \mu(1-\mu^2)g^2\frac{dg}{d\mu}\right)\frac{\partial c_0}{\partial \eta} - \frac{\partial^2 c_0}{\partial \eta^2} = 0. \quad (43)$$

Provided there is a solution in which the term in large parentheses is equal to a constant,

$$g^3 - \mu(1-\mu^2)g^2\frac{dg}{d\mu} = \Delta, \quad (44)$$

the governing equation becomes

$$\frac{\partial c_0}{\partial \chi} + \beta\Delta\eta^2\frac{\partial c_0}{\partial \eta} - \frac{\partial^2 c_0}{\partial \eta^2} = 0. \quad (45)$$

Without loss of generality, we make the choice $\Delta = 1$. The differential equation for $g(\mu)$ is easily solved, with Υ a constant of integration,

$$g(\mu) = \left(1 + \Upsilon\frac{\mu^3}{(1-\mu^2)^{\frac{3}{2}}}\right)^{\frac{1}{3}}. \quad (46)$$

We require that $g(\mu)$ be bounded, except at the poles $\mu = \pm 1$ where the boundary layer scaling may break down. As a result, we make the choice $\Upsilon = 1$ for $\mu \geqslant 0$ and $\Upsilon = -1$ for $\mu < 0$.

Before tackling the first-passage problem, we highlight the physics of the concentration boundary layer by considering the steady-state solution ($\frac{\partial c_0}{\partial \chi} = 0$) for the concentration profile in the presence of a perfectly absorbing sphere ($c_0 = 0$ at $\eta = 0$) with toxin concentration c_∞ far away from the sphere (see Figs. 5 and 6). The solution is readily obtained in terms of the incomplete Gamma function $\Gamma(a,z)$ as

$$c_0 = c_\infty\left(1 - \frac{\Gamma\left(\frac{1}{3}, \frac{\beta}{3}\eta^3\right)}{\Gamma\left(\frac{1}{3}\right)}\right), \quad (47)$$

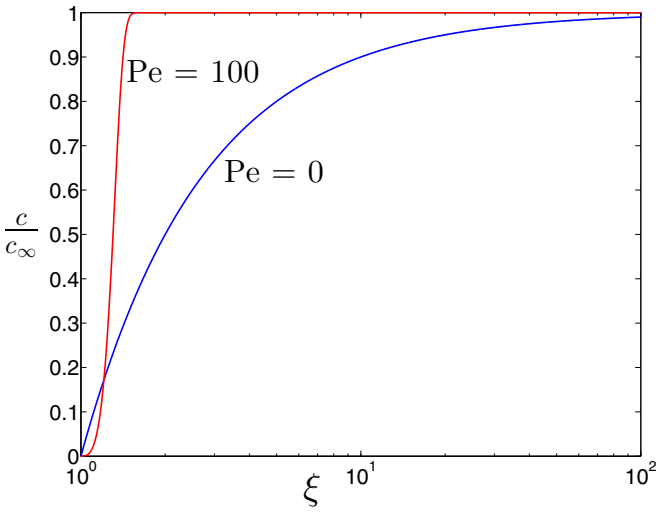

FIG. 5. (Color online) The steady-state concentration profile c/c_∞, normalized by the far-field concentration c_∞, as a function of the dimensionless radial variable ξ. The case of pure diffusion (Pe = 0), Eq. (69), is shown as a blue line. The concentration profile (along the line $\theta = \pi/4$) in the advection-dominated regime (Pe = 100), Eq. (47), is shown as a red line.

$$\Gamma(a,z) = \int_z^\infty t^{a-1}e^{-t}dt. \quad (48)$$

To quantify the mass transfer from the sphere in the case of strong advection, we calculate the zeroth-order result for the dimensionless Sherwood number,

$$\mathrm{Sh}_0 = \frac{1}{4\pi c_\infty}\int_0^\pi \sin\theta\, d\theta \int_0^{2\pi} d\phi \left.\frac{\partial c_0}{\partial \xi}\right|_{\xi=1}. \quad (49)$$

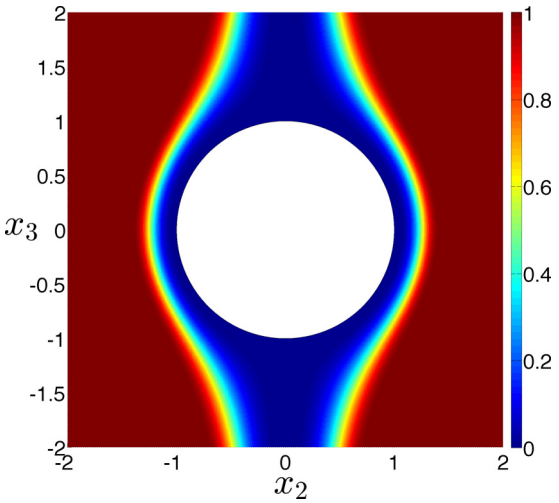

FIG. 6. (Color online) Steady-state concentration contours of c/c_∞ in the (x_2,x_3) plane for the case of strong advection (Pe = 100). Note the thickness of the concentration-boundary layer. The concentration rapidly approaches its far-field value ($c/c_\infty = 1$) in a thin layer surrounding the embryo.

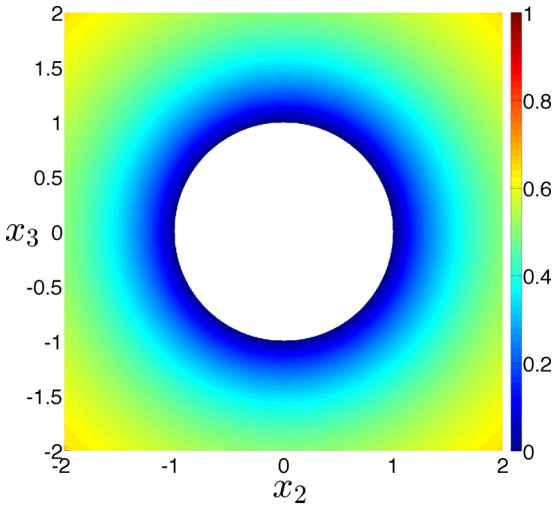

FIG. 7. (Color online) Steady-state concentration contours of c/c_∞ in the (x_2,x_3) plane for the case of pure diffusion (Pe = 0). Note the thickness of the concentration-boundary layer. At twice the embryo radius, the concentration has approached roughly half of its far-field value ($c/c_\infty = 1$).

Using the above results, we find

$$\mathrm{Sh}_0 = \left(\frac{3^{\frac{2}{3}}\beta^{\frac{1}{3}}\mathcal{I}}{2\,\Gamma(\frac{1}{3})}\right)\mathrm{Pe}^{\frac{1}{3}} \approx 0.59\,\mathrm{Pe}^{\frac{1}{3}}, \tag{50}$$

$$\mathcal{I} = \int_{-1}^{1}\frac{d\mu}{g(\mu)} \approx 1.66. \tag{51}$$

Based on the mathematical equivalence of the mass and heat transfer problems, Eq. (50) can be compared to the result of Acrivos and Taylor for the dependence of the Nusselt number Nu on the Péclet number Pe [23]. The exponent 1/3 is the same in both cases, but the dimensionless prefactor differs (0.99 versus 0.59), which is unsurprising since the fluid models are not the same in the two cases. Acrivos and Taylor also report the leading-order corrections to this result for small Reynolds number Re, whereas in the present section we restrict our attention to the case Re = 0.

Defined in the same manner, $\mathrm{Sh}_D = 1$ for the case of pure diffusion (Pe = 0), which can be readily obtained using the appropriate diffusive concentration profile $c = c_\infty(1-\frac{1}{\xi})$ for the given boundary conditions (see Fig. 7). This highlights the advective enhancement of mass transfer away from the sphere $\sim \mathrm{Pe}^{\frac{1}{3}}$ at $\mathrm{Pe} \gg 1$, with the exponent 1/3 coming from the boundary layer analysis.

V. THE CASE OF STRONG ADVECTION

We now consider the first-passage problem for the case of strong advection. For the purposes of the present calculation, we consider a spatial domain where all toxin molecules released at the tips of microvilli are eventually captured with probability 1. To do so, consider two perfectly absorbing surfaces, the first at the surface of the spherical embryo ($\eta = 0$), and a second at some prescribed distance ($\eta = \eta_+$). We define the time-integrated concentration

$$\mathcal{C}_0 = \int_0^\infty c_0\, d\chi. \tag{52}$$

The equation governing $\mathcal{C}_0$ becomes

$$c_0(\chi=\infty) - c_0(\chi=0) + \beta\eta^2\frac{\partial \mathcal{C}_0}{\partial \eta} - \frac{\partial^2 \mathcal{C}_0}{\partial \eta^2} = 0. \tag{53}$$

Since all toxin molecules are absorbed with probability 1, $c_0(\chi=\infty) = 0$. The initial condition corresponding to a point source at the microvilli tip is $c_0(\chi=0) = \delta^3(\vec{\xi}-\vec{\xi}')$. By considering the sequence of variable transformations introduced earlier, $(\xi,\tau)\to(\rho,T)\to(\eta,\chi)$, and transforming the initial condition, we arrive at the governing equation,

$$\frac{\partial^2 \mathcal{C}_0}{\partial \eta^2} - \beta\eta^2\frac{\partial \mathcal{C}_0}{\partial \eta} = -\frac{\delta\left(\eta - \frac{g(\mu')}{g(\mu)}\eta'\right)\delta(\mu-\mu')\delta(\phi-\phi')}{\alpha^{\frac{1}{3}}g(\mu)(1+\alpha^{\frac{1}{3}}g(\mu)\eta)^2}. \tag{54}$$

The two independent solutions to the homogeneous equation [right-hand side of Eq. (54) = 0] are a constant $\mathcal{C}_0^{(1)} = \kappa$, and the incomplete Gamma function $\mathcal{C}_0^{(2)} = \Gamma(\frac{1}{3},\frac{\beta}{3}\eta^3)$. The solution for $\mathcal{C}_0$ with absorbing boundary conditions can evidently be written in the form

$$\mathcal{C}_0 = Q\left[\Gamma\left(\frac{1}{3},\frac{\beta}{3}\eta_<^3\right) - \Gamma\left(\frac{1}{3}\right)\right] \times\left[\Gamma\left(\frac{1}{3},\frac{\beta}{3}\eta_>^3\right) - \Gamma\left(\frac{1}{3},\frac{\beta}{3}\eta_+^3\right)\right]. \tag{55}$$

Here $\eta_<$ ($\eta_>$) is the smaller (larger) of η and η'. To determine the constant Q, we integrate both sides of the governing equation $\int_{-1}^{1}d\mu\int_0^{2\pi}d\phi\int_{\eta=\eta'-\epsilon}^{\eta=\eta'+\epsilon}d\eta$ to determine the discontinuity in the first derivative of $\mathcal{C}_0$,

$$4\pi\left.\frac{\partial \mathcal{C}_0}{\partial \eta}\right|_{\eta=\eta'-\epsilon}^{\eta=\eta'+\epsilon} = -\frac{1}{\alpha^{\frac{1}{3}}g(\mu')(1+\alpha^{\frac{1}{3}}g(\mu')\eta')^2}. \tag{56}$$

A short calculation gives

$$Q = -\frac{e^{\frac{\beta}{3}(\eta')^3}}{4\pi\,3^{\frac{2}{3}}(\beta\alpha)^{\frac{1}{3}}\left[\Gamma\left(\frac{1}{3}\right) - \Gamma\left(\frac{1}{3},\frac{\beta}{3}(\eta_+)^3\right)\right]g(\mu')(1+\alpha^{\frac{1}{3}}g(\mu')\eta')^2}. \tag{57}$$

The first-passage probability is calculated from the concentration as

$$\Pi_0 = \int_0^\infty d\tau\int_{-1}^{1}d\mu\int_0^{2\pi}d\phi\left.\frac{\partial c_0}{\partial \xi}\right|_{\xi=1}. \tag{58}$$

Making the same sequence of variable transformations introduced earlier, the result can be written in terms of the time-integrated concentration $\mathcal{C}_0$ as

$$\Pi_0 = \alpha^{\frac{1}{3}}\int_{-1}^{1}d\mu\int_0^{2\pi}d\phi\left.\frac{\partial \mathcal{C}_0}{\partial \eta}\right|_{\eta=0}g(\mu). \tag{59}$$

The result of the angular integration gives

$$\Pi_0 = \frac{e^{\frac{\beta}{3}(\eta')^3}\Gamma(\frac{1}{3},\frac{\beta}{3}(\eta')^3)\mathcal{J}}{2\left[\Gamma\left(\frac{1}{3}\right)-\Gamma(\frac{1}{3},\frac{\beta}{3}(\eta_+)^3)\right]g(\mu')(1+\alpha^{\frac{1}{3}}g(\mu')\eta')^2}, \tag{60}$$

$$\mathcal{J} = \int_{-1}^{1} d\mu\, g(\mu) \approx 2.97. \tag{61}$$

The result of the calculation can be greatly simplified by changing back to our original variables, and noting that $e^z\,\Gamma(\frac{1}{3},z) \approx z^{-\frac{2}{3}} + O(z^{-\frac{4}{3}})$ for $z \gg 1$. This approximation is justified in our case since $\alpha = 1/\mathrm{Pe} \ll 1$ and therefore $z = \frac{\beta(\xi'-1)^3}{3\alpha g(\mu')^3} \gg 1$. Taking the outer absorbing surface to infinity, $\eta_+ \to \infty$, we arrive at the final result:

$$\Pi_0 \approx \left(\frac{3^{\frac{2}{3}}\mathcal{J}}{2\Gamma(\frac{1}{3})\beta^{\frac{2}{3}}}\right)\frac{g(\mu')}{(\xi')^2(\xi'-1)^2}\,\mathrm{Pe}^{-\frac{2}{3}} + O(\mathrm{Pe}^{-\frac{4}{3}}). \tag{62}$$

The result can be interpreted simply as follows. The first term in parentheses is a dimensionless number of order unity, $(\frac{3^{\frac{2}{3}}\mathcal{J}}{2\Gamma(\frac{1}{3})\beta^{\frac{2}{3}}}) \approx 0.94$, which depends on the properties of the microscale velocity gradient ($\beta = \frac{15}{2}\langle \mathsf{e}_{33}\rangle$) and the angular dependence of the concentration boundary layer thickness (through $\mathcal{J}$). The second term gives the dependence of the first-passage probability on the location (μ') and length (ξ') of the microvillus that releases the toxin. The last term gives the dependence of the first-passage probability on the Péclet number $\sim \mathrm{Pe}^{-\frac{2}{3}}$. Note the dramatic reduction (see Fig. 8) of the first-passage probability as compared to the earlier case of diffusive transport (Pe = 0), for which $\Pi_D = 1/\xi'$.

Comparing to the result in the case of pure diffusion, Eq. (7), we see that in the advection-dominated regime, the first-passage probability is reduced as compared to the purely diffusive first capture probability. One can continue the perturbation program by calculating more of the $\{c_k\}$ and the leading-order corrections to the first-passage probability. Provided that $\alpha^{\frac{1}{3}} = \mathrm{Pe}^{-\frac{1}{3}}$ is small, these corrections will not change the qualitative result of the zeroth-order calculation.

The drastic reduction of uptake probability for microvilli lengths in quantitative agreement with experimental measurements of microvilli structure supports a functional significance to tip localization of toxin transporters. When viewed through the lens of the toxin transport problem, one might say that the microvilli length has been evolutionarily selected to probe the thickness of the concentration boundary layer. Toxin molecules released at the tips of microvilli will be advected away from the embryo, decreasing the probability that they will be reabsorbed and have to be exported again, which is energetically costly for the embryo. Within the biological transporter literature, this sequence of export and subsequent reabsorption is referred to as futile cycling [29].

Within the present first-passage formalism, we can quantify the cost associated with futile cycling of toxin molecules. The cost to the embryo to efflux a single toxin molecule is two molecules of ATP. As a result, the average number of ATP consumed to efflux a single toxin molecule is

$$\langle N_{\mathrm{ATP}}\rangle = \sum_{n=1}^{\infty} 2n\Pi^{n-1}(1-\Pi) = \frac{2}{1-\Pi}. \tag{63}$$

As demonstrated in Fig. 9, the effect of reducing the absorption probability is compounded when computing the cost of the transporter system for the embryo, with a significant reduction

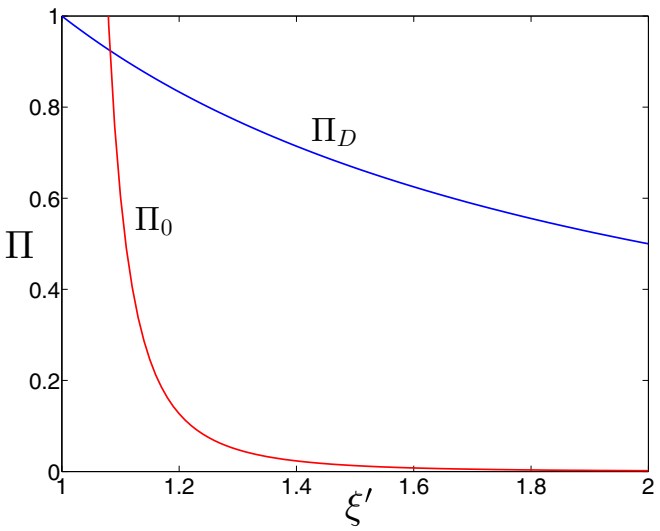

FIG. 8. (Color online) The first-passage probability Π as a function of the microvilli tip location ξ'. The result for the case of pure diffusion (Pe = 0), Π_D, is shown as a blue line. The zeroth-order result for the case of strong advection (Pe = 2062), Π_0, is shown as a red line. Note that in the advection-dominated case, the values of ξ' over which there is a rapid decrease in absorption probability agree quite well with the length of embryonic microvilli. Microvilli of height $h = 2$, 5, and 10 μm correspond to $\xi' = 1.05$, 1.125, and 1.25, respectively.

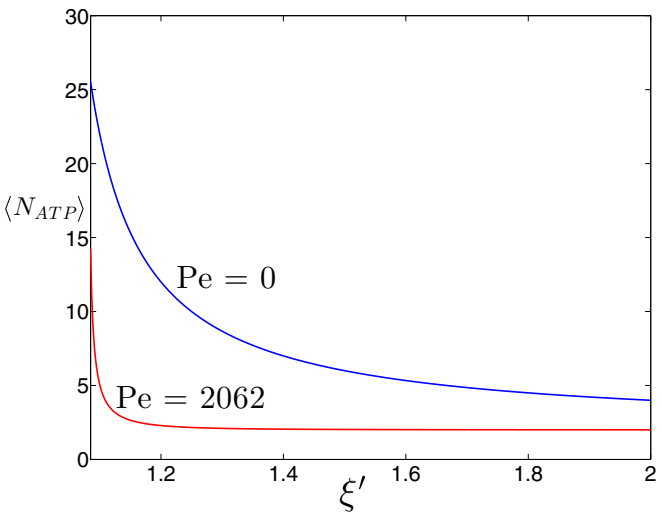

FIG. 9. (Color online) The average number of ATP molecules $\langle N_{\mathrm{ATP}}\rangle$ required to efflux a single toxin molecule as a function of the microvilli tip location ξ'. The result for the case of pure diffusion (Pe = 0) is shown as a blue line. The zeroth-order result for the case of strong-advection (Pe = 2062) is shown as a red line.

in the energy budget for the transporter system provided by the enhanced mass transport at large Pe.

VI. SURFACE ROUGHNESS

Thus far in our discussion, the role of the microvilli has been simply to displace the toxin above the surface of the embryo, where it is subsequently released into the extracellular fluid. In our calculations of the first-passage probability, we have only considered absorption on the smooth spherical surface of the embryo. In this approximation, the *phantom* microvilli do not contribute to the surface area available for absorption, and they do not modify the fluid flow in the vicinity of the embryo. In this section, we discuss how modifying these assumptions might affect the first-passage probabilities.

To begin, we collect some results about the microvillar architecture during sea urchin embryogenesis [see Figs. 10(a) and 10(b)]. The microvilli are solitary, unbranched, cylindrical cell membrane protrusions. There is substantial heterogeneity in the length of microvilli on the sea urchin embryo, with at least two populations of microvilli [30,31]. The short microvilli (SMV) have a length of $h_{\rm SMV} \simeq 2$–$3\ \mu$m, comparable to the thickness of the hyaline layer that surrounds the embryo [6,32]. The elongated microvilli (EMV) are substantially longer, spanning the perivitelline space between the embryo surface and the fertilization envelope. Their length depends on the width of the perivitelline space, in *Strongylocentrotus purpuratus* $h_{\rm EMV} \simeq 35\ \mu$m. The radius $\varrho \simeq 0.1\ \mu$m of the microvilli is the same for both populations (SMV and EMV). According to studies on *Strongylocentrotus droebachiensis*, there are $N \approx 3 \times 10^5$ microvilli covering the embryo [31].

The presence of microvilli increases the effective surface area of the embryo available for absorption, and as a result it should increase the first-passage probability. The embryo's

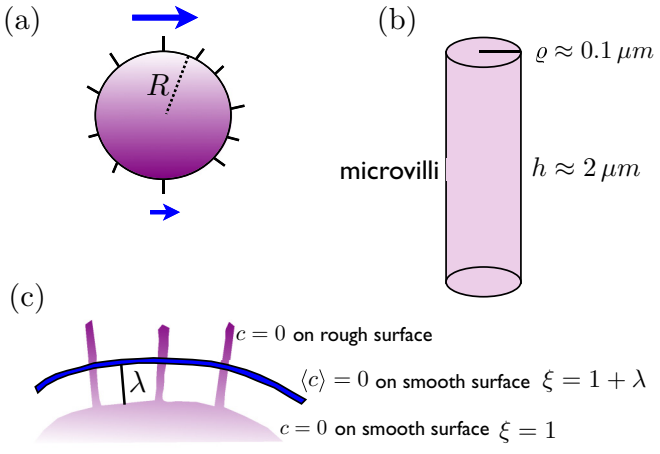

FIG. 10. (Color online) (a) Hundreds of thousands of microvilli (short lines) roughen the surface of a spherical embryo of radius $R \approx 40\ \mu$m in a microscale velocity gradient (blue arrows). (b) Schematic of an individual microvillus, a cylindrical cell membrane protrusion of radius $\varrho \approx 0.1\ \mu$m and length $h \approx 2\ \mu$m. (c) In the multiple scattering calculation, the effect of surface roughness is to displace the smooth surface by a distance λ.

total surface area is

$$A_{\rm embryo} = 4\pi R^2 + N(2\pi\varrho h). \tag{64}$$

The first contribution is from the smooth spherical surface, and the second takes into account the cylindrical microvilli with average length h. For an embryo with radius $R = 40\ \mu$m, the smooth surface provides an area of $2.0 \times 10^4\ \mu$m^2. With an average length of $h = 2\ \mu$m, the microvilli provide an area of $3.8 \times 10^5\ \mu$m^2. The result is that a rough embryo has a surface area at least 20 times as large as its smooth counterpart.

To calculate the effect of surface roughness on the first-passage probability presents a significant challenge. The technical problem is how the absorbing boundary condition can be applied on the rough surface. An analytic approach to related problems has been developed based on ideas from multiple scattering theory [33]. In principle, the idea is to replace the exact boundary condition for the concentration c on the rough surface (in our case the Dirichlet condition $c = 0$ on the rough surface) by an effective boundary condition for the ensemble-averaged concentration $\langle c \rangle_{\rm rough}$ on the underlying smooth surface [34]. The subscript "rough" has been utilized so as not to confuse this averaging procedure with the temporal average utilized earlier in the paper for the computation of the fluid velocity. The ensemble-averaged concentration is defined as

$$\langle c \rangle_{\rm rough}(\vec{\xi}\,) = \frac{1}{N!} \int d\mathcal{C}_N\ P(\mathcal{C}_N)\, c(\vec{\xi}\,|N). \tag{65}$$

The notation $c(\vec{\xi}\,|N)$ emphasizes that the concentration depends not only on the position $\vec{\xi}$ but also on the configuration of the microvilli. The averaging procedure is with respect to all possible arrangements of the microvilli on the smooth spherical surface. Each arrangement of the microvilli is called a *configuration* denoted by $\mathcal{C}_N \equiv (\vec{Y}_1, \vec{Y}_2, \ldots, \vec{Y}_N)$. Here $\vec{Y}_i$ denotes the position of the base of microvillus i with respect to a curvilinear coordinate system on the smooth surface. The normalization is defined by

$$N! = \int d\mathcal{C}_N\ P(\mathcal{C}_N) = \int d^2\vec{Y}_1 \cdots \int d^2\vec{Y}_N\ P(\mathcal{C}_N), \tag{66}$$

with a configuration appearing in the ensemble with probability $P(\mathcal{C}_N)$. The theory has been worked out in detail for the case of Laplace's equation [34], $\nabla^2_{\vec{\xi}} c = 0$, which is the same as the steady-state diffusion equation. The main result is an effective boundary condition for the ensemble-averaged concentration, which, for a uniform spatial distribution of microvilli, takes the form

$$\langle c \rangle_{\rm rough}\Big|_{\xi=1} = -\lambda \frac{\partial \langle c \rangle_{\rm rough}}{\partial \xi}\Big|_{\xi=1}. \tag{67}$$

Note that the effect of surface roughness is to introduce a new length scale in the problem through the effective boundary condition. The physical interpretation of λ is a measure of the displacement of the $\langle c \rangle_{\rm rough} = 0$ surface above the smooth surface, as shown in Fig. 10(c). In other words, if the Dirichlet boundary condition $c = 0$ applies at the smooth surface $\xi = 1$, the effect of surface roughness is to impose the condition $\langle c \rangle_{\rm rough} = 0$ at the surface $\xi = 1 + \lambda$. Introducing the fraction of the smooth surface covered by the microvilli, $\varphi = \frac{N\pi\varrho^2}{4\pi R^2}$, the

dimensionless length

$$\lambda = (1+k)\varphi\frac{h}{R}. \tag{68}$$

Here k is a dimensionless number that depends in general on φ. In the dilute limit, $\varphi \ll 1$, k depends only on the shape of the microvilli.

As an example to illustrate the potential effect of surface roughness, consider the solution of Laplace's equation $\nabla_\xi^2 c = 0$ for the dimensionless concentration c, with the Dirichlet boundary condition $c(\xi = 1) = 0$. If the far-field boundary condition is a constant concentration c_∞, the solution is readily obtained as

$$c = c_\infty\left(1 - \frac{1}{\xi}\right). \tag{69}$$

The dimensionless Sherwood number is calculated as

$$\mathrm{Sh}_D = \frac{1}{4\pi c_\infty}\int_0^\pi \sin\theta\, d\theta \int_0^{2\pi} d\phi \left.\frac{\partial c}{\partial \xi}\right|_{\xi=1} = 1. \tag{70}$$

To determine the effect of surface roughness, consider the related problem for the ensemble-averaged concentration $\langle c\rangle_{\mathrm{rough}}$, with the Dirichlet boundary condition replaced by Eq. (67). We calculate the concentration

$$\langle c\rangle_{\mathrm{rough}} = c_\infty\left(1 - \frac{1}{1-\lambda}\frac{1}{\xi}\right). \tag{71}$$

The result for the Sherwood number is then

$$\langle \mathrm{Sh}_D\rangle_{\mathrm{rough}} = \frac{1}{1-\lambda}. \tag{72}$$

The increase of toxin current density impinging on the rough sphere should translate into an increase in the first-passage probability. Unfortunately, a direct application of these results to the first-passage problem is somewhat problematic, since the effective boundary condition Eq. (67) is specific to the homogeneous Laplace equation. For the first-passage application, we would need results for Poisson's equation (for the case of pure diffusion), and the equation governing $\mathcal{C}_0$ (for the advection-dominated regime). An interesting avenue for future research is to extend the work of [34] to the present first-passage formalism.

In what follows, we consider a slightly more heuristic approach to capturing the effect of surface roughness. Recall that the effective boundary condition can be interpreted as displacing the Dirichlet boundary condition above the smooth surface. This suggests that we might be able to capture the effect of surface roughness by increasing the radius of the embryo and decreasing the length of the microvilli,

$$R_{\mathrm{rough}} = R + \lambda R, \tag{73}$$

$$h_{\mathrm{rough}} = h - \lambda R. \tag{74}$$

Considering our earlier result for the diffusive first-passage probability, $\Pi_D = 1/\xi'$, and recalling $\xi' = 1 + \frac{h}{R}$, after rescaling we find

$$\langle \Pi_D\rangle_{\mathrm{rough}} = \frac{1}{\xi'_{\mathrm{rough}}} = \frac{(1+\lambda)}{\xi'} = (1+\lambda)\,\Pi_D. \tag{75}$$

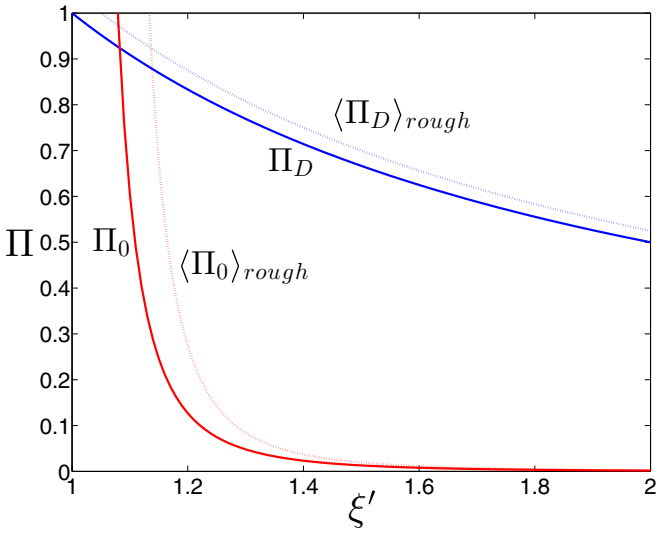

FIG. 11. (Color online) The first-passage probability Π as a function of the microvilli tip location ξ'. The effect of surface roughness is to increase the first-passage probability. Heuristic estimates for the magnitude of the effect are provided by the dashed lines.

This result is in agreement with our calculation of the Sherwood number, which suggests enhancement by the factor $1/(1-\lambda)$, with deviations at $O(\lambda^2)$. By performing the same rescaling (see Fig. 11), a naive extension to our result in the advection-dominated regime suggests that

$$\langle \Pi_0\rangle_{\mathrm{rough}} \approx \left(\frac{3^{\frac{2}{3}}\mathcal{J}}{2\Gamma\left(\frac{1}{3}\right)\beta^{\frac{2}{3}}}\right)\frac{g(\mu')}{\left(\frac{\xi'}{1+\lambda}\right)^2\left(\frac{\xi'}{1+\lambda}-1\right)^2}\,\mathrm{Pe}^{-\frac{2}{3}} + O(\mathrm{Pe}^{-\frac{4}{3}}). \tag{76}$$

To determine λ, we first calculate the surface fraction $\varphi \approx 0.47$. This is not so small so as to safely rely on the dilute results for k, so as a first approximation we consider the numerical results derived at finite φ. Note that the numerics are for the case of hemispherical microvilli [34]. We find $1 + k \approx 1.93$ and $\lambda \approx 0.05$.

We caution the reader that the discussion above is somewhat speculative, since the effective boundary condition Eq. (67) is specific to the homogeneous Laplace equation. An interesting avenue for future research is to extend the work of [34] to the present first-passage formalism. This would entail deriving an effective boundary condition similar to Eq. (67) for the inhomogeneous equations governing the concentration. Multiple scattering methods have also been applied to the problem of determining the disturbance in the flow field produced by surface roughness elements [35]. The ensemble averaged flow field could then be utilized as input for the advection-diffusion equation to capture the effect of the microvilli on modifying the flow in the vicinity of the embryo surface. This is a significant task for future research.

VII. CONCLUSIONS

In this paper, we considered a spherical embryo of radius $R \sim 40\ \mu$m in a flow-field with characteristic velocity $U_0 \sim R/\tau_\eta$ as is typical for the smallest eddies in a turbulent

macroscale flow. The diffusion coefficient of the toxin in the extracellular fluid is $D \sim 10^{-5}$ cm^2 s^{-1}. The dimensionless Péclet number, which characterizes the competition between advection and diffusion, is

$$\mathrm{Pe} = \frac{RU_0}{D} \gg 1. \tag{77}$$

This means that relative to transport of the toxin in the extracellular fluid, advection is much more important than diffusion. In this regime of large Pe, a concentration boundary layer forms near the embryo. The boundary layer length scales as

$$\ell = R\,\mathrm{Pe}^{-\frac{1}{3}}. \tag{78}$$

This gives a boundary layer of several microns in thickness. Interestingly, this agrees quite well with the microvilli length, and it would provide a physical reason for a distribution of transporters localized on the tips of the microvilli. At the tips of the microvilli, the toxin concentration approaches the far-field value. Toxins released at this height will be advected away from the embryo before having a chance to diffuse to the surface and be internalized. The major result of the paper, Eq. (62), is illustrated in Fig. 8. The argument is that the tip-localized transporter distribution and the microvilli architecture are evolutionarily adapted to probe the thickness of the concentration boundary layer. The success and efficiency of the multidrug transporters rely crucially on the presence of fluid flow in the open ocean environment of the sea urchin embryo. Ignorant of the biochemical details of the transporter system, the physics governing mass transport at large Péclet number provides a compelling reason for the observed length of embryonic microvilli during sea urchin development.

A number of simplifications have been made in the present paper. For the purposes of building a tractable model system that does not obscure the underlying physics, many details of sea urchin biology have been stripped away, including the presence of the hyaline layer surrounding the embryo and the fertilization envelope. We have not considered how the microvilli will alter the fluid flow in the vicinity of the embryo. Further work, in a computational fluid dynamics framework, could address these issues and incorporate a spatially varying toxin diffusivity. Incorporating details of the chemical kinetics of the transporter system would pose a challenging problem of reaction, advection, and diffusion in a heterogeneous media.

The primary message from the paper on the relationship between the length scale of surface roughness elements and the mass transport problem is likely applicable beyond the scope of sea urchin development. Villi are ubiquitous structures in biology [36], and similar ideas will carry over in other settings with a gradient in fluid velocity. The design of a diverse variety of transport and mechanosensory systems may be guided by similar underlying principles [4], from toxin export by aquatic organisms residing in the benthic boundary layer [13,37], to mechanotransduction by epithelial cells in the kidney [38].

ACKNOWLEDGMENTS

This work was supported by a College of Arts, Sciences, and Letters Faculty Summer Research Grant from the University of Michigan–Dearborn. N.L. acknowledges support from National Science Foundation Award PHY-0645652 while at Indiana University, during early stages of this work, as well as insightful discussions with Sima Setayeshgar about biophysical aspects of toxin transport in the sea urchin embryo that motivated this work.

APPENDIX A: THE CASE OF PURE DIFFUSION (PE = 0)

This appendix outlines the solution for the first-passage probability in the purely diffusive case, where Pe = 0. Using the completeness relation for the δ function in spherical polar coordinates,

$$\delta^3(\vec{\xi}-\vec{\xi}') = \frac{1}{\xi^2}\delta(\xi-\xi')\sum_{\ell=0}^{\infty}\sum_{m=-\ell}^{\ell} Y^*_{\ell m}(\theta',\phi')Y_{\ell m}(\theta,\phi), \tag{A1}$$

and inserting the expansion Eq. (4) into Eq. (3) yields the radial equation

$$\frac{d^2a_{\ell m}}{d\xi^2} + \frac{2}{\xi}\frac{da_{\ell m}}{d\xi} - \frac{\ell(\ell+1)}{\xi^2}a_{\ell m} - \gamma^2 a_{\ell m} = -\frac{1}{\xi^2}\delta(\xi-\xi'). \tag{A2}$$

Here we have defined $\gamma^2 = s$. Making the substitution $a_{\ell m} = \frac{b_{\ell m}}{(\gamma\xi)^{1/2}}$, the radial equation becomes

$$\xi^2\frac{d^2b_{\ell m}}{d\xi^2} + \xi\frac{db_{\ell m}}{d\xi} - \left[\left(\ell+\frac{1}{2}\right)^2 + (\gamma\xi)^2\right]b_{\ell m} = -(\gamma\xi)^{\frac{1}{2}}\delta(\xi-\xi'). \tag{A3}$$

As is evident from the form of the differential equation, the homogeneous solutions for the $b_{\ell m}$ are the modified Bessel functions of order $\ell+\frac{1}{2}$, denoted by $I_{\ell+\frac{1}{2}}(\gamma\xi)$ and $K_{\ell+\frac{1}{2}}(\gamma\xi)$. The solution to Eq. (A3) which is finite at infinity is

$$b_{\ell m}(\xi,\xi') = K_{\ell+\frac{1}{2}}(\gamma\xi_>)[AI_{\ell+\frac{1}{2}}(\gamma\xi_<) + BK_{\ell+\frac{1}{2}}(\gamma\xi_<)]. \tag{A4}$$

Here $\xi_<$ ($\xi_>$) represents the smaller (larger) of ξ and ξ'. The absorbing boundary condition $b_{\ell m} = 0$ at the surface of the embryo $\xi = 1$ is satisfied by the choice $B = -A\frac{I_{\ell+\frac{1}{2}}(\gamma)}{K_{\ell+\frac{1}{2}}(\gamma)}$. The remaining constant $A = (\frac{\gamma}{\xi'})^{1/2}$ is determined by integrating Eq. (A3) from $\xi = \xi' - \epsilon$ to $\xi = \xi' + \epsilon$ and noting that the Wronskian of the modified Bessel functions is given by

$$I_{\ell+\frac{1}{2}}(x)\frac{dK_{\ell+\frac{1}{2}}(x)}{dx} - \frac{dI_{\ell+\frac{1}{2}}(x)}{dx}K_{\ell+\frac{1}{2}}(x) = -\frac{1}{x}. \tag{A5}$$

Hence the solution for the $b_{\ell m}$ is

$$b_{\ell m}(\xi,\xi') = \left(\frac{\gamma}{\xi'}\right)^{\frac{1}{2}} K_{\ell+\frac{1}{2}}(\gamma\xi_>) \times\left(I_{\ell+\frac{1}{2}}(\gamma\xi_<) - \frac{I_{\ell+\frac{1}{2}}(\gamma)}{K_{\ell+\frac{1}{2}}(\gamma)}K_{\ell+\frac{1}{2}}(\gamma\xi_<)\right). \tag{A6}$$

We define the spherical modified Bessel functions $i_\ell(x) = \sqrt{\frac{\pi}{2x}}I_{\ell+\frac{1}{2}}(x)$ and $k_\ell(x) = \sqrt{\frac{2}{\pi x}}K_{\ell+\frac{1}{2}}(x)$. Note that the numerical factors in the definitions of $i_\ell(x)$ and $k_\ell(x)$ differ [12]. Making this substitution above and recalling the relation

$a_{\ell m} = \frac{b_{\ell m}}{(\gamma\xi)^{1/2}}$, the solution to Eq. (A2) is Eq. (5) from the main text,

$$a_{\ell m}(\xi,\xi') = \gamma k_\ell(\gamma\xi_>)\left[i_\ell(\gamma\xi_<) - \frac{i_\ell(\gamma)}{k_\ell(\gamma)}k_\ell(\gamma\xi_<)\right]. \quad \text{(A7)}$$

To calculate the first-passage probability

$$\Pi_D = \int_0^\infty dt \iint \vec{J}\cdot\vec{da}, \quad \text{(A8)}$$

note that the current density $\vec{J} = -D\vec{\nabla}C$ and $\vec{da} = -\hat{r}\,R^2\sin\theta\,d\theta\,d\phi$. Moving to the dimensionless variables introduced earlier, the equation can be written as

$$\Pi_D = \lim_{s\to 0}\int_0^\infty e^{-s\tau} J(\tau)\,d\tau = \lim_{s\to 0}\tilde{j}(s), \quad \text{(A9)}$$

$$J(\tau) = \int_0^\pi \sin\theta\,d\theta \int_0^{2\pi} d\phi \left.\frac{\partial c}{\partial\xi}\right|_{\xi=1}. \quad \text{(A10)}$$

This establishes that the first-passage probability can be calculated from the Laplace transform of the current $\tilde{j}(s)$ by taking the limit that $s \to 0$. We calculate

$$\tilde{j}(s) = \sum_{\ell=0}^\infty\sum_{m=-\ell}^{\ell}\gamma k_\ell(\gamma\xi')\left(\frac{\partial i_\ell(\gamma\xi)}{\partial\xi} - \frac{i_\ell(\gamma)}{k_\ell(\gamma)}\frac{\partial k_\ell(\gamma\xi)}{\partial\xi}\right)\Bigg|_{\xi=1} \times Y^*_{\ell m}(\theta',\phi')\int_0^\pi \sin\theta\,d\theta\int_0^{2\pi} d\phi\,Y_{\ell m}(\theta,\phi). \quad \text{(A11)}$$

As a result of the angular integration $\int_0^\pi \sin\theta\,d\theta\int_0^{2\pi} d\phi\,Y_{\ell m}(\theta,\phi) = \sqrt{4\pi}\delta_{\ell,0}\delta_{m,0}$, the only nonzero term has $\ell = m = 0$. Using the fact that $i_0(x) = \sinh(x)/x$ and $k_0(x) = e^{-x}/x$, a short calculation gives

$$\tilde{j}(s) = \frac{e^{-\gamma(\xi'-1)}}{\xi'}. \quad \text{(A12)}$$

Recalling that $\gamma^2 = s$ and taking the limit that $s \to 0$ of the above expression yields the final result quoted in the main text,

$$\Pi_D = \frac{1}{\xi'}. \quad \text{(A13)}$$

APPENDIX B: THE CASE OF STRONG ADVECTION (PE ≫ 1)

This appendix provides details necessary for the solution for the first-passage probability in the case of strong advection, where Pe $\gg 1$. Defining a spherical polar coordinate system with the x_3 axis along the direction of the ambient vorticity, the Cartesian components of the antisymmetric part of the velocity gradient tensor take the form $\Omega_{ij} = -\frac{1}{2}\epsilon_{ij3}\omega$. The spherical polar components are calculated as

$$\begin{pmatrix}\Omega_{rr} & \Omega_{r\theta} & \Omega_{r\phi}\\ \Omega_{\theta r} & \Omega_{\theta\theta} & \Omega_{\theta\phi}\\ \Omega_{\phi r} & \Omega_{\phi\theta} & \Omega_{\phi\phi}\end{pmatrix} = \begin{pmatrix}\sin\theta\cos\phi & \sin\theta\sin\phi & \cos\theta\\ \cos\theta\cos\phi & \cos\theta\sin\phi & -\sin\theta\\ -\sin\phi & \cos\phi & 0\end{pmatrix} \times \begin{pmatrix}0 & -\frac{\omega}{2} & 0\\ \frac{\omega}{2} & 0 & 0\\ 0 & 0 & 0\end{pmatrix} \times \begin{pmatrix}\sin\theta\cos\phi & \cos\theta\cos\phi & -\sin\phi\\ \sin\theta\sin\phi & \cos\theta\sin\phi & \cos\phi\\ \cos\theta & -\sin\theta & 0\end{pmatrix} = \frac{\omega}{2}\begin{pmatrix}0 & 0 & -\sin\theta\\ 0 & 0 & -\cos\theta\\ \sin\theta & \cos\theta & 0\end{pmatrix}. \quad \text{(B1)}$$

The spherical polar components of the symmetric part of the velocity gradient tensor E can be calculated in a similar fashion from the Cartesian components, which satisfy $\mathsf{E}_{ij} = \mathsf{E}_{ji}$. Moving to a frame of reference that is rotating with the embryo by making the replacement $\phi \to \phi - \mathrm{Pe}\,\tau$, the leading contributions to the time-averaged velocity components expressed in terms of the radial variable ρ are

$$\langle u^*_\xi\rangle = \left[\tfrac{15}{2}\rho^2\alpha^{\frac{2}{3}} - 20\rho^3\alpha + O(\alpha^{\frac{4}{3}})\right]\langle \mathsf{e}_{33}\rangle, \quad \text{(B2)}$$

$$\langle u^*_\theta\rangle = \left[-\tfrac{15}{4}\rho\alpha^{\frac{1}{3}} + \tfrac{15}{2}\rho^2\alpha^{\frac{2}{3}} - 15\rho^3\alpha + O(\alpha^{\frac{4}{3}})\right] \times \sin(2\theta)\langle \mathsf{e}_{33}\rangle, \quad \text{(B3)}$$

$$\langle u^*_\phi\rangle = 0. \quad \text{(B4)}$$

[1] H. C. Berg and E. M. Purcell, Physics of chemoreception, Biophys. J. **20**, 193 (1977).

[2] H. C. Berg, *Random walks in biology* (Princeton University Press, Princeton, NJ, 1993).

[3] R. E. Goldstein, in *Biological physics* (Springer, Basel, 2011), pp. 123–139.

[4] M. B. Short, C. A. Solari, S. Ganguly, T. R. Powers, J. O. Kessler, and R. E. Goldstein, Flows driven by flagella of multicellular organisms enhance long-range molecular transport, Proc. Natl. Acad. Sci. (U.S.A.) **103**, 8315 (2006).

[5] S. Vogel, *Life in moving fluids: The physical biology of flow* (Princeton University Press, Princeton, NJ, 1994).

[6] K. Whalen, A. M. Reitzel, and A. Hamdoun, Actin polymerization controls the activation of multidrug efflux at fertilization by translocation and fine-scale positioning of ABCB1 on microvilli, Mol. Biol. Cell **23**, 3663 (2012).

[7] T. Gökirmak, J. P. Campanale, L. E. Shipp, G. W. Moy, H. Tao, and A. Hamdoun, Localization and substrate selectivity of sea urchin multidrug (MDR) efflux transporters, J. Biol. Chem. **287**, 43876 (2012).

[8] K. Lange and J. Gartzke, Microvillar cell surface as a natural defense system against xenobiotics: A new interpretation of multi drug resistance, Am. J. Physiol.-Cell Physiol. **281**, C369 (2001).

[9] K. Lange, Fundamental role of microvilli in the main functions of differentiated cells: Outline of an universal regulating and signaling system at the cell periphery, J. Cell. Physiol. **226**, 896 (2011).

[10] S. Redner, *A guide to first-passage processes* (Cambridge University Press, Cambridge, 2001).

[11] Xianfeng Song, Ph.D. thesis, Indiana University, 2008.

[12] G. B. Arfken, H.-J. Weber, and L. Ruby, *Mathematical methods for physicists* (Academic, New York, 1985), Vol. 6.

[13] K. S. Mead and M. W. Denny, The effects of hydrodynamic shear stress on fertilization and early development of the purple sea urchin strongylocentrotus purpuratus, Biol. Bull. **188**, 46 (1995).

[14] M. Denny, J. Dairiki, and S. Distefano, Biological consequences of topography on wave-swept rocky shores: I. Enhancement of external fertilization, Biol. Bull. **183**, 220 (1992).

[15] J. Lazier and K. Mann, Turbulence and the diffusive layers around small organisms, Deep Sea Res. Pt. A: Oceanogr. Res. Pap. **36**, 1721 (1989).

[16] L. Karp-Boss, E. Boss, and P. A. Jumars, Nutrient fluxes to planktonic osmotrophs in the presence of fluid motion, Oceanogr. Marine Biol.: An Ann. Rev. **34**, 71 (1996).

[17] E. Berdalet and M. Estrada, Effects of small-scale turbulence on the physiological functioning of marine microalgae, in *Algal Cultures, Analogues of Blooms and Applications*, edited by D. V. Subba Rao (Science Publishers, New Hampshire, USA, 2005), Vol. 2, pp. 459–499.

[18] S. B. Pope, *Turbulent flows* (Cambridge University Press, Cambridge, 2000).

[19] G. K. Batchelor, Mass transfer from a particle suspended in fluid with a steady linear ambient velocity distribution, J. Fluid Mech. **95**, 369 (1979).

[20] G. K. Batchelor, Mass transfer from small particles suspended in turbulent fluid, J. Fluid Mech. **98**, 609 (1980).

[21] K. McDonald, Patterns in early embryonic motility: Effects of size and environmental temperature on vertical velocities of sinking and swimming echinoid blastulae, Biol. Bull. **207**, 93 (2004).

[22] A. Lévêque, *Les Lois de la Transmission de Chaleur par Convection* (Dunod, Paris, 1928).

[23] A. Acrivos and T. D. Taylor, Heat and Mass Transfer from Single Spheres in Stokes Flow, Phys. Fluids **5**, 387 (1962).

[24] M. Van Dyke, *Perturbation methods in fluid mechanics* (Academic, New York, 1964), Vol. 964.

[25] L.-Y. Chen, N. Goldenfeld, and Y. Oono, Renormalization group and singular perturbations: Multiple scales, boundary layers, and reductive perturbation theory, Phys. Rev. E **54**, 376 (1996).

[26] I. John Veysey and N. Goldenfeld, Simple viscous flows: From boundary layers to the renormalization group, Rev. Mod. Phys. **79**, 883 (2007).

[27] V. Magar, T. Goto, and T. Pedley, Nutrient uptake by a self-propelled steady squirmer, Q. J. Mech. Appl. Math. **56**, 65 (2003).

[28] V. Magar and T. Pedley, Average nutrient uptake by a self-propelled unsteady squirmer, J. Fluid Mech. **539**, 93 (2005).

[29] B. J. Cole, A. Hamdoun, and D. Epel, Cost, effectiveness and environmental relevance of multidrug transporters in sea urchin embryos, J. Exp. Biol. **216**, 3896 (2013).

[30] E. Spiegel, L. Howard, and M. Spiegel, Elongated microvilli support the sea urchin embryo concentrically within the perivitelline space until hatching, Roux's Archives Develop. Biol. **198**, 85 (1989).

[31] T. E. Schroeder, Microvilli on sea urchin eggs: A second burst of elongation, Develop. Biol. **64**, 342 (1978).

[32] E. Spiegel, L. Howard, and M. Spiegel, The contractility of elongated microvilli in early sea urchin embryos, Roux's Archives Develop. Biol. **199**, 228 (1990).

[33] L. L. Foldy, The multiple scattering of waves. I. General theory of isotropic scattering by randomly distributed scatterers, Phys. Rev. **67**, 107 (1945).

[34] K. Sarkar and A. Prosperetti, Effective Boundary Conditions for the Laplace Equation with a Rough Boundary, Proc. R. Soc. London, Ser. A **451**, 425 (1995).

[35] K. Sarkar and A. Prosperetti, Effective boundary conditions for Stokes flow over a rough surface, J. Fluid Mech. **316**, 223 (1996).

[36] A. Kultti, K. Rilla, R. Tiihonen, A. P. Spicer, R. H. Tammi, and M. I. Tammi, Hyaluronan Synthesis Induces Microvillus-like Cell Surface Protrusions, J. Biol. Chem. **281**, 15821 (2006).

[37] K. Bowden, Physical problems of the benthic boundary layer, Geophys. Surv. **3**, 255 (1978).

[38] P. Guo, A. M. Weinstein, and S. Weinbaum, A hydrodynamic mechanosensory hypothesis for brush border microvilli, Am. J. Physiol.-Renal Physiol. **279**, F698 (2000).